Aerodynamic Limits on Large Civil Tiltrotor Sizing and Efficiency

C. W. Acree, Jr.
Aeromechanics Office
National Aeronautics and Space Administration
Ames Research Center, Moffett Field, California
Cecil.W.Acree@NASA.gov

Abstract

The NASA Large Civil Tiltrotor (2nd generation, or LCTR2) is a useful reference design for technology impact studies. The present paper takes a broad view of technology assessment by examining the extremes of what aerodynamic improvements might hope to accomplish. Performance was analyzed with aerodynamically idealized rotor, wing, and airframe, representing the physical limits of a large tiltrotor. The analysis was repeated with more realistic assumptions, which revealed that increased maximum rotor lift capability is potentially more effective in improving overall vehicle efficiency than higher rotor or wing efficiency. To balance these purely theoretical studies, some practical limitations on airframe layout are also discussed, along with their implications for wing design. Performance of a less efficient but more practical aircraft with non-tilting nacelles is presented.

Notation

A	rotor disk area
b	inner wing span
c	chord
c_{do}	section profile drag coefficient
c_l	section lift coefficient
c_m	section moment coefficient
C_T	rotor thrust coefficient, $T/(\rho A V_{tip}^2)$
C_W	rotor weight coefficient, $W/(\rho A V_{tip}^2)$
D	drag
d_x	wing extension span
e	span efficiency factor
e_x	wing extension offset
FM	figure of merit
$F_{q\dot{q}}$	damping force
k	modal stiffness
L	lift
L/D_e	aircraft lift over equivalent drag, WV/P
M	pitching moment
m	modal mass
P	power required
ρ	atmospheric density
q	dynamic pressure; generalized mode shape
Q_A	generalized aerodynamic force
Q_B	integrated bending force
Q_T	integrated torsion force
T	rotor thrust
V	airspeed
V_{br}	aircraft best-range speed

V_{tip}	rotor tip speed
W	gross weight
WE	weight empty
x, y, z	linear coordinate axes
ϕ	torsion mode axis
α	angle of attack
γ	torsion mode shape
δ	modal damping
η	propulsive efficiency, TV/P
κ	induced velocity factor
Λ	extension sweep angle
σ	rotor solidity (thrust-weighted)
ζ	beamwise mode shape

AVL	Athena Vortex Lattice
CAMRAD	Comprehensive Analytical Model of Rotorcraft Aerodynamics and Dynamics
CRP	Contingency Rated Power
ISA	International Standard Atmosphere
LCTR2	Large Civil Tilt Rotor—2nd generation
MCP	Maximum Continuous Power
MRP	Maximum Rated Power (take-off power)
NDARC	NASA Design and Analysis of Rotorcraft
NPSS	Numerical Propulsion System Simulation
OEI	One Engine Inoperative
OGE	Out of Ground Effect
SFC	Specific Fuel Consumption
SNI	Simultaneous Non-Interfering approach
WATE	Weight Analysis of Turbine Engines

Introduction

The NASA Large Civil Tiltrotor (2nd generation, or LCTR2) has been the reference design for a variety of NASA studies of design optimization, engine and gearbox technology, handling qualities, and other areas, with contributions from NASA Ames, Glenn and Langley Centers, plus academic and industry studies. Ongoing work includes airfoil design, 3D blade optimization, engine technology studies, and wing/rotor aerodynamic interference. The original concept was developed as part of the NASA Heavy Lift Rotorcraft Systems Investigation (Ref. 1), and has since evolved into the second-generation LCTR2, described in detail in Refs. 2 and 3; further evolution of the design provided by engine technology is discussed in Refs. 4 and 5. The LCTR2 is designed to carry 90 passengers for 1,000 nm at 300 knots, with vertical takeoff and landing (Fig. 1). The overall purpose of the design effort is to develop a consistent basis for evaluating the benefits of advanced technology for large tiltrotors.

In parallel with the work reported here, additional research related to advanced tiltrotors with direct relevance to LCTR2 is underway. In particular, studies of wing/rotor aerodynamic interaction and of aeroelastic effects of wing extensions are reported in Refs. 6 and 7 respectively. References 6 and 7 go into much greater depth in their particular areas of focus than the more general studies reported herein. Multiparameter optimization of proprotors is reported in Ref. 8; the goal of that research is a new LCTR2 rotor design. Wind-tunnel tests of an LCTR2 airframe model (Ref. 9) will provide better aerodynamic data for handling qualities research. The data will also be used to update the aerodynamic model used for sizing studies.

The purpose of the present paper is two-fold: 1) determine where future technology studies might have the greatest payoff, and 2) establish a stronger basis of comparison for studies of other vehicle configurations and missions. In addition, practical constraints on vehicle layout are considered, which leads directly to aerodynamic redesign of the wing. The effects of wing extensions on aeroelastic stability are included in the redesign, here on a purely conceptual basis.

This paper first describes the LCTR2 aircraft and mission, and summarizes the analytical methods use to construct performance models used for sizing. Next are presented results of assuming idealized rotor and wing performance on the LCTR2 design, along with a more conventional sensitivity study. The practical benefits of fixed engines and wing extensions (that is, non-tilting) are discussed; this leads directly to aerodynamic redesign of the wing. An Appendix introduces the theoretical justification for the use of swept extensions to improve stability margins for whirl flutter.

Aircraft and Mission

Table 1 and Fig. 2 summarize the LCTR2 mission requirements. Category A OEI is modeled as occurring at 20 knots forward airspeed, which incorporates lessons from XV-15 flight tests (Refs. 10-12, summarized in Ref. 4). The climb to cruise altitude is modeled as two equal-height segments for better trim convergence during sizing. Most recently, a 250-knot limit below 10,000 ft was added, although this had little effect on the results.

Table 2 lists key constraints and assumptions imposed during the design. The three "minimum performance" constraints are the most important for sizing. In addition, the blade loading limit is a fallout of the 80-knot banked turn requirement (Table 1). The 80-knot turn represents an emergency maneuver and was analyzed in detail in Ref. 13, which derived the blade loading limit. The disk loading and wing loading were optimized in Ref. 14.

The LCTR2 design assumes an advanced turboshaft engine combined with a two-speed gearbox to achieve optimum rotor tip speed in cruise while retaining low fuel consumption (good engine specific fuel consumption, or SFC). More advanced engine concepts, focusing on variable-speed turbines, were studied in Refs. 4 and 5; see also Ref. 15. However, the increased engine efficiency was insufficient to compensate for the higher engine weight. Therefore, an advanced engine with conventional power turbine layout was assumed for the present study. The engine model assumes technology available in 2035, and is discussed in detail in Refs. 16 and 17.

The LCTR2 drive train utilizes a pair of compound planetary gearboxes, one for each rotor, with a speed changing module at each input. Each module is a conventional clutched planetary gearbox. See Ref. 15 for details, including shift strategy.

Hover tip speed is set by noise considerations. Cruise tip speed was optimized in Ref. 4 and represents a tradeoff between rotor efficiency, engine efficiency, and drive-train weight. The trends are nearly flat near the optimum, and some studies (Ref. 15) have favored a higher cruise tip speed than that used here. Different assumptions of airfoil, engine and gearbox technology could easily change the optimum tip speed. For this paper, the lower value of 350 ft/s was chosen to take advantage of the benefits of wing/rotor aerodynamic interactions.
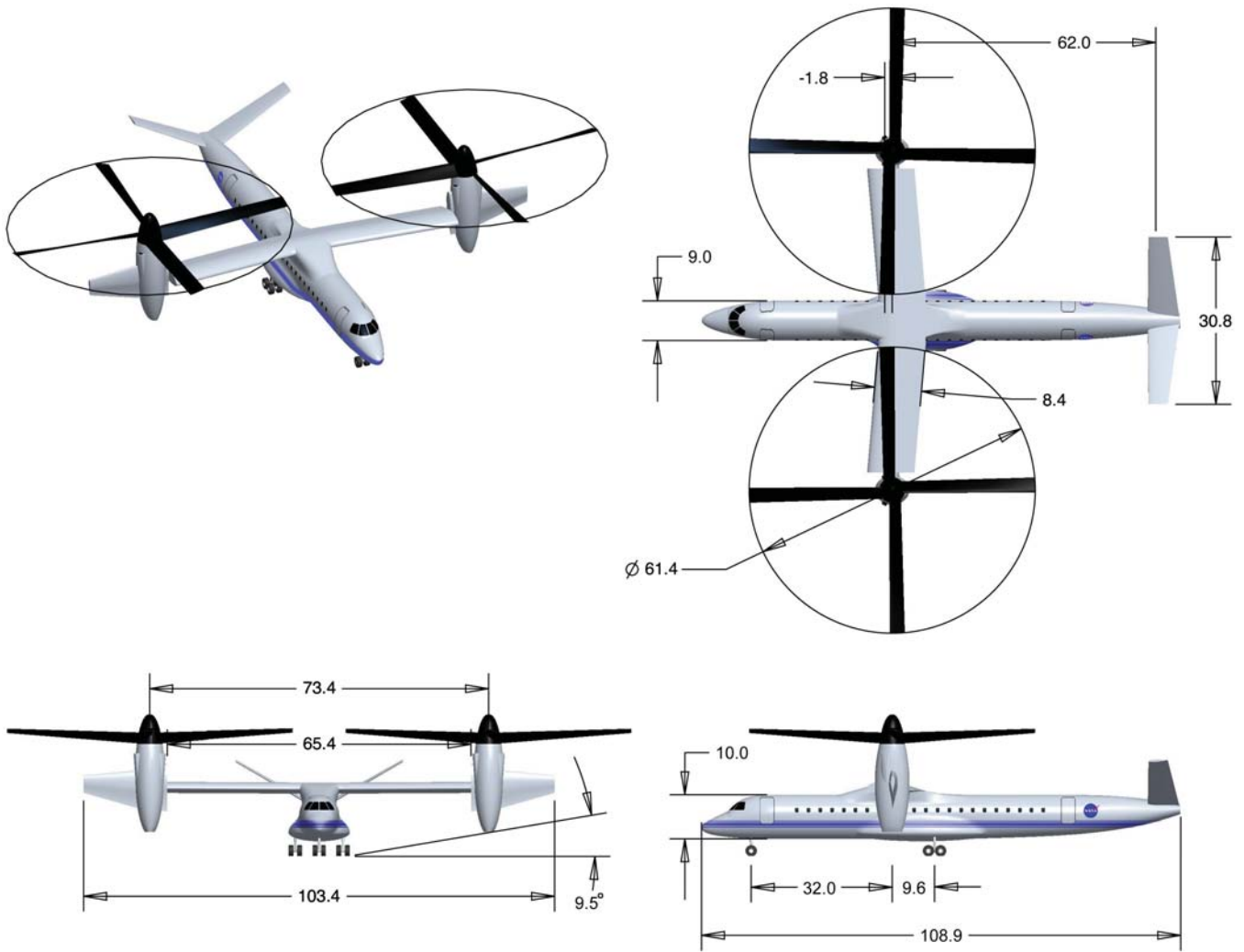
Fig. 1. The NASA Large Civil Tiltrotor, LCTR2 baseline version as resized with NDARC Release 1.7 (dimensions in feet).
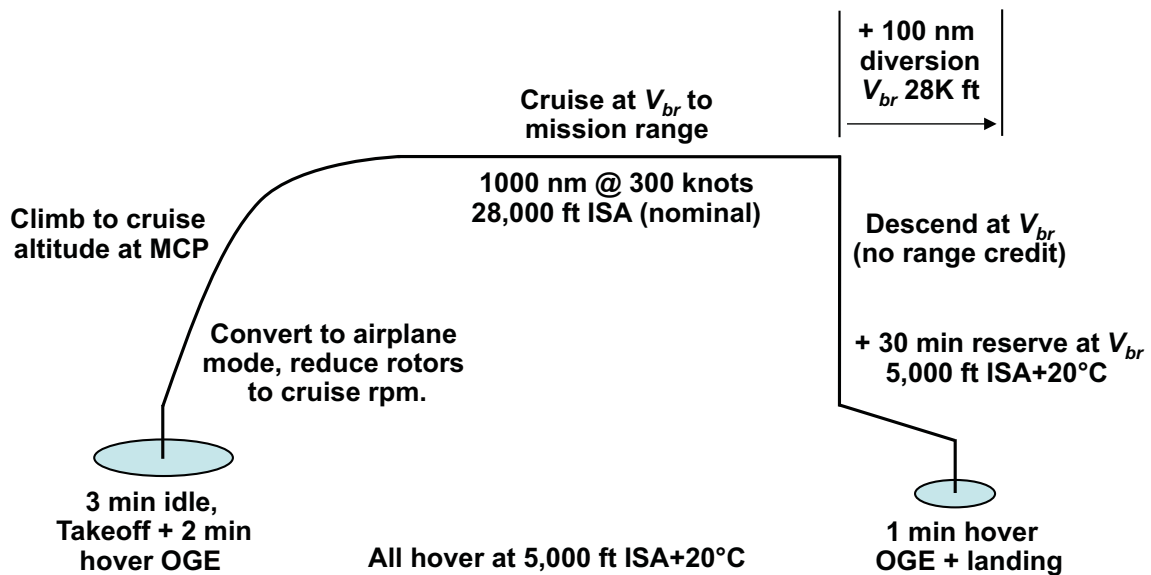

Fig. 2. LCTR2 mission profile.

Table 1. LCTR2 mission requirements.

Mission summary
Takeoff + 2 min hover OGE 5k ISA+20°C
Climb at V_{br} (credit distance to cruise segment)
Cruise at V_{br} for at least 1,000 nm range, 28k ISA
Descend at V_{br} (no range credit)
1 min hover OGE + landing, 5k ISA+20°C
Reserve (diversion): 100 nm V_{br}, 28k ISA
Reserve (emergency): 30 min V_{br}, 5k ISA+20°C

Operational requirements
One engine inoperative: Category A at 5k ISA+20°C
All-weather operations: CAT IIIC SNI, Free Flight
45-deg banked turn at 80 knots, 5k ISA+20°C, 90% MCP

Table 2. LCTR2-03 design constraints for sizing.

Minimum Performance	
Max. takeoff weight at sea level standard, 100% MRP	
OEI at 5k ISA+20°C, 20 knots, 100% CRP	
Cruise speed 300 knots at 28k ISA, 90% MCP	
Design Constraints	
Payload (90 pax), lb	19,800
Cruise speed (90% MCP), knots	300
Fuselage diameter, ft	9.0
Length, ft	108.9
Wing span, ft	107.0
Wing sweep (inboard), deg	−5.0
Rotor radius, ft (max)	32.5
Number of blades	4
Precone, deg	6.0
Key Technology Assumptions	
Wing loading, lb/ft^2	105
Disk loading, lb/ft^2	14
[a]Hover blade loading C_W/σ	0.151
[b]Cruise SFC, lb/hr/hp	0.3255
[c]Tip speed, hover, ft/s	650
[d]Tip speed, cruise, ft/s	350

[a]Set by maneuver requirement

[b]Advanced Conventional Engine spec.

[c]Set by assumed future noise requirements

[d]Determined by previous analyses

Analytical Tools

For the LCTR2, aerodynamic optimization typically proceeds in three steps: (1) the isolated rotor, at a fixed sized, is optimized with CAMRAD II; (2) the optimized rotor is combined with a wing, and the total vehicle performance, including aerodynamic interference and non-axial flow, is determined with CAMRAD II; and (3) the rotor and wing performance so determined is input into NDARC, which sizes the aircraft. Previously developed structural and engine models were also incorporated into NDARC. The following paragraphs describe the analytical tools in more detail.

The present study used the design code NDARC (NASA Design and Analysis of Rotorcraft, Release 1.7, Refs. 18-20). The rotor performance model used within NDARC was developed with CAMRAD II (Comprehensive Analytical Model of Rotorcraft Aerodynamics and Dynamics, Refs. 21-22); Refs. 2 and 3 describe the development of the model in some detail. Wing performance was determined by Athena Vortex Lattice (AVL), developed by Mark Drela and Harold Youngren and available from MIT (Ref. 22). The method of combining AVL and CAMRAD II predictions is described in the section Wing Design. NPSS (Numerical Propulsion System Simulation, Ref. 23) and WATE (Weight Analysis of Turbine Engines, Ref. 24) were previously used to develop the NDARC engine model, as described in Refs. 16 and 17.

The rotor performance predicted with CAMRAD II was based on the assumed performance of advanced airfoils and included the effects of wing/rotor interference, as described in Ref. 2. The CAMRAD II results were represented within the NDARC rotor model as equivalent values of rotor profile and induced drag, each varying with the flight conditions specified in Table 1 and Fig. 2.

Rotor performance is further influenced by wing/rotor interaction, and wing efficiency is strongly affected by the rotor wake (Refs. 2 and 25; see also Ref. 26). CAMRAD II was used to analyze all of these effects using a model with a wake for each rotor and the wing (Ref. 27). The CAMRAD II results were captured in algebraic rotor and wing performance models for efficient computation within NDARC.

The blade twist was always set to the classic helix twist angle, which is a very close approximation to the optimum twist distribution determined in Ref. 2. A small improvement in hover performance is possible with a revised twist distribution, but for a long-range aircraft, cruise efficiency is paramount and dominates the sizing process via fuel burn. Installed power is determined by OEI requirements. Blade loading and disk loading requirements (Table 2) directly affect hover performance. While better hover performance is always useful if it can be attained without compromising cruise efficiency, maximizing hover efficiency was not critical for the LCTR2 mission. However, the results reported here suggest that better turn performance might be even more useful than hover or cruise efficiency, which would require a different optimization method than used heretofore.

At the beginning of each sizing analysis, the rotor radius was set to 32.5 ft, and the wing area to 1020 ft^2. NDARC then adjusted rotor radius and wing chord to meet the required values of disk loading and wing loading. Rotor solidity was adjusted to match the constraint on blade loading until sizing converged.

Ideal Performance

NDARC is a convenient tool for exploring the limits of achievable efficiency. Wing and rotor efficiencies can be described in terms of profile and induced drag. The analyses presented here are based on the concept of an "ideal" rotor with figure of merit (FM) and propulsive efficiency (η) both equal to unity. FM and η may be further broken down into induced and profile power components. Induced power can be represented by the induced velocity factor κ, where from momentum theory $\kappa = 1$ is the minimum possible induced velocity, hence minimum possible induced power. Profile power results from profile drag c_{do}, where the minimum value is zero. NDARC can set either κ or c_{do} to their minimum values for hover and cruise separately. Similar analyses can be performed for the wing, where hover download, profile drag, and induced drag can be separately set to their minimum values. Airframe drag can be separated into nacelle and fuselage contributions.

Figure 3 summarizes the results of applying different combinations of ideal wing and rotor performance to LCTR2 sizing. The values in the figure represent the physical limits of what LCTR2 might be capable of, given advanced technology (such as, for example, a hyper-morphing rotor that always has ideal lift distribution). Weight empty, mission fuel burn, and installed power are all shown as percentages of the baseline values of Ref. 4, as updated with NDARC Release 1.7 and listed in Table 3. Values less than 100% are accordingly improvements. The vertical scale of Fig. 3 is adjusted to better reveal the effects of specific improvements to drag or efficiency. "Ideal Cruise" applies $\kappa = 1$, $c_{do} = 0$, or both to cruise conditions only; "Ideal Hover" similarly applies to hover only. The "FM, η" bars include ideal values of both κ and c_{do}, hence $FM = 1$ and $\eta = 1$ simultaneously. Similar plots are shown for the wing, where the "Ideal Wing" bars include minimum values of download, induced drag and profile drag simultaneously. The plotted results are obviously unrealistic, in that they represent the extremes of what is physically possible. Further improvement would require changes to the LCTR2 configuration itself.

Scanning across the columns immediately reveals the changes with the largest improvements in each category (weight, fuel or power). Improvements to rotor performance almost always have a greater effect than improvements to the wing.

The single largest improvement in all categories results from a reduction in rotor induced power (κ) in hover, which leads to a very large decrease in installed power. The engine is sized by the OEI requirement at near-hover conditions, not by 300-knot cruise at altitude. A smaller engine improves fuel consumption, hence empty weight. Hence installed power, fuel burn and empty weight all benefit more from improvements to rotor hover performance than to cruise performance. This result implies that LCTR2 cruise performance might be usefully traded off against hover performance. However, the idealization assumes that induced power in hover can be reduced to the ideal value without any adverse effect on cruise performance (see Fig. 4 for a more realistic assessment).

It is not surprising that reductions in profile drag (c_{do}), for the airframe yield the next largest improvement, seen as a decrease in fuel consumption. In contrast, zero vertical drag has almost no effect. The LCTR2 mission does not include sustained hover (only 3 minutes total), and the 20-knot OEI requirement essentially eliminates download at that condition. Therefore, reductions in download have little effect on LCTR2 sizing. The results would differ for a tiltrotor with an extended hover requirement.

A very large reduction in engine size is theoretically achievable. Note that this applies to any type of propulsion system and represents the limit imposed by the aerodynamics of the vehicle, not the thermodynamics (or electrodynamics) of the engine. Reductions in empty weight are limited by the fixed fuselage size needed to carry 90 passengers, hence one would expect to see relatively larger reductions in engine size and fuel consumption.

However, Fig. 3 does not tell the whole story. The LCTR2 is required to have enough reserve performance to achieve a 45-deg banked turn at 80 knots (5k ISA+20°C, 90% MCP conditions). This requirement sets the maximum allowable blade loading C_{Tmax}/σ (i.e., a stall limit; see Ref. 13).

There is no well-defined ideal for stall corresponding to the momentum theory limits of $FM = 1$ or $\eta = 1$, so there is no direct comparison to Fig. 3. To evaluate the effect of increased stall boundary relative to other possible improvements, a series of matched parameter variations were carried out on profile and induced drag for the wing, rotor and fuselage, and on solidity. Reducing solidity is equivalent to increasing blade loading. Selected efficiency parameters in the NDARC performance model were each reduced by 10% from the baseline model previously established by CAMRAD II analyses.

Rotor profile drag and solidity were set to 90% of the nominal values, as were wing profile drag and airframe drag. The minimum possible value for rotor induced drag can be represented as $\kappa = 1$, and the minimum possible wing induced drag yields a maximum induced efficiency $e = 1$ (for a wing without interference). To ensure the adjusted induced drag values did not exceed these limits, the 10% reduction was made to the non-ideal components: $\kappa' = 1 + 0.1(\kappa - 1)$ and $e' = 1 - 0.1(1 - e)$. This approach provides a consistent basis for comparison, with the further benefit of yielding profile and induced drag values less outlandish than zero or unity. Figure 4 presents the results of 10% improvements to component efficiencies and to C_{Tmax}/σ. The vertical scales have been shifted to highlight the effects of individual contributions.
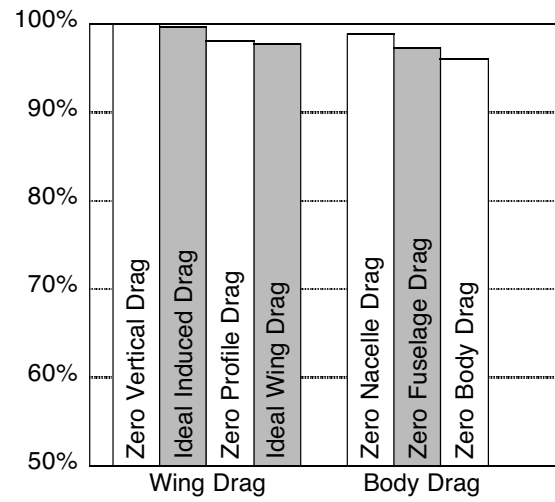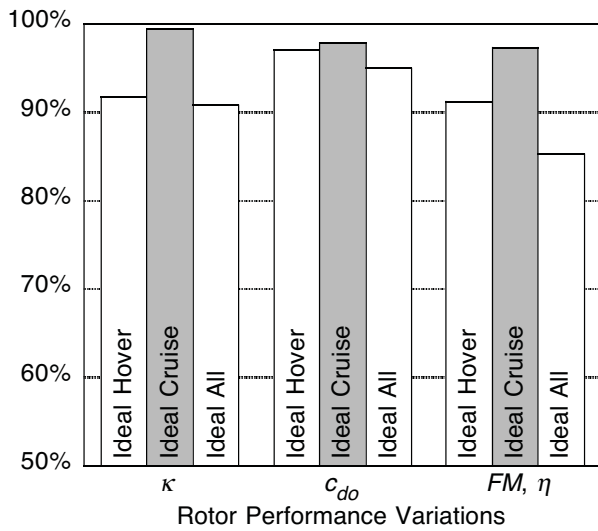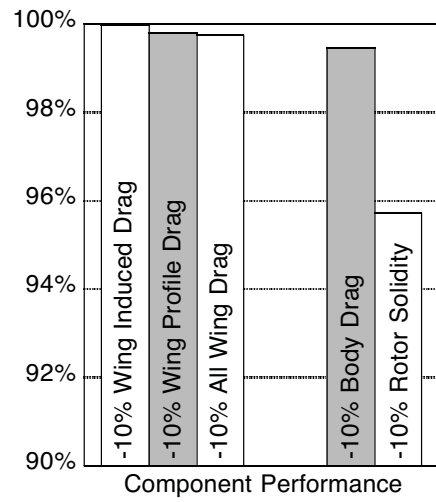
(a) Weight empty
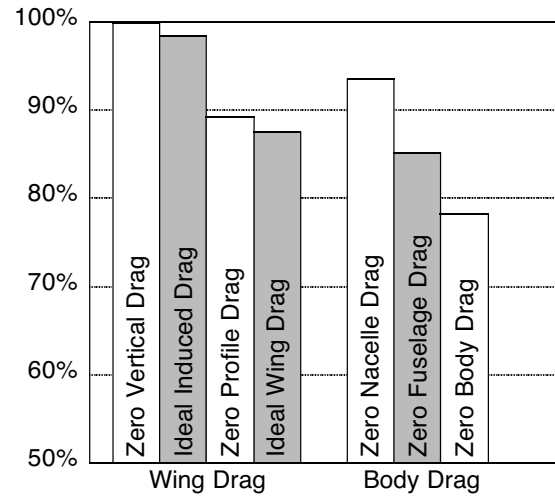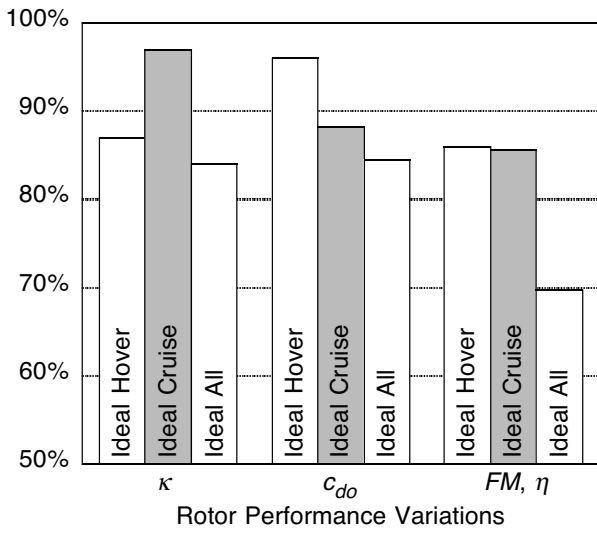
(b) Mission fuel burn
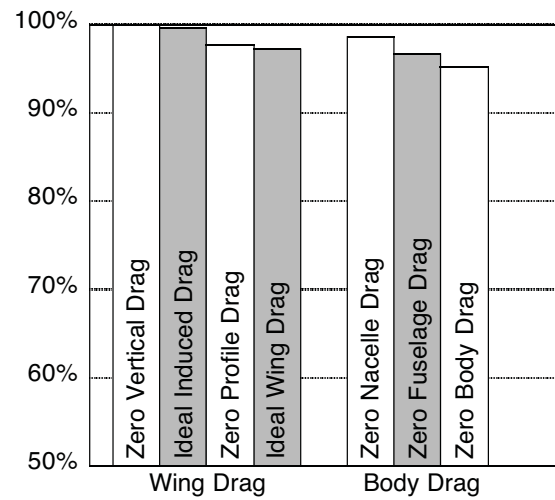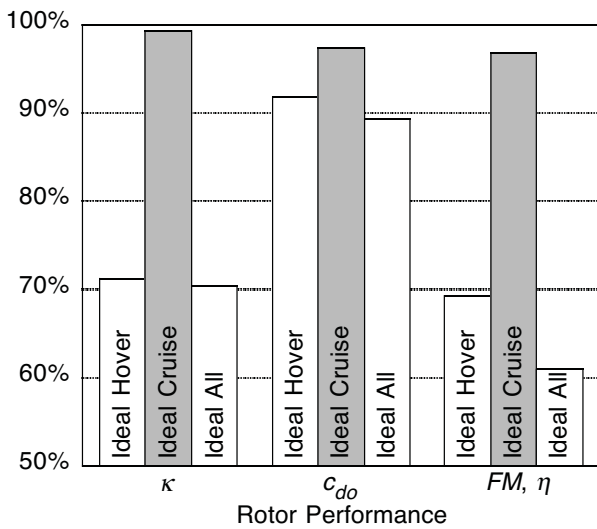
(c) Installed power

Fig. 3. Impact of ideal rotor and airframe performance on LCTR2 design. Ideal rotor performance is shown on the left; ideal wing and fuselage performance is on the right.
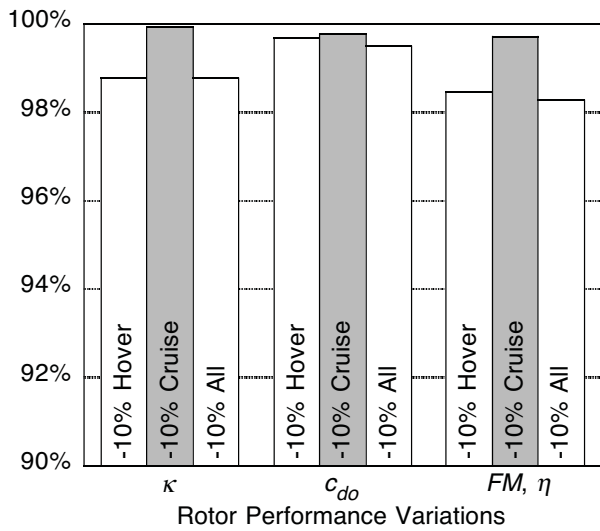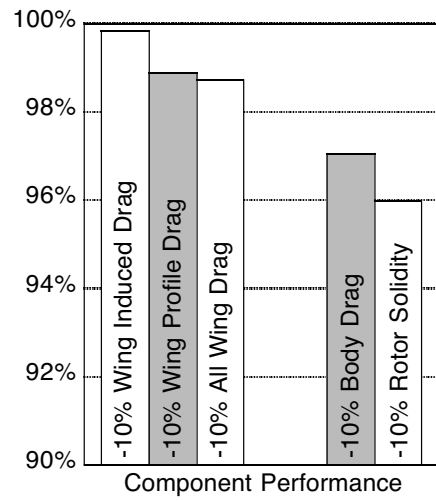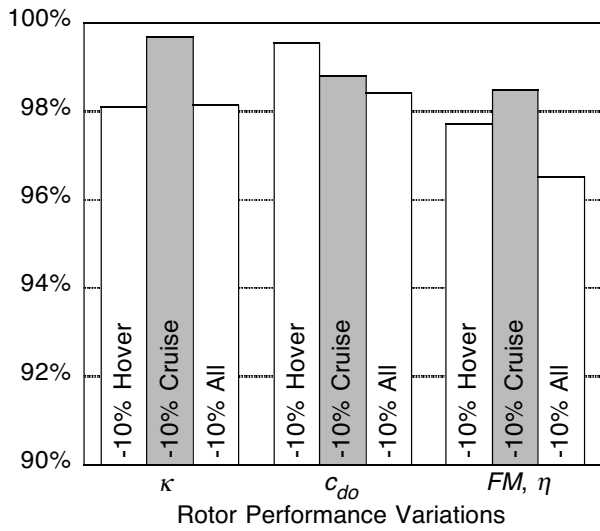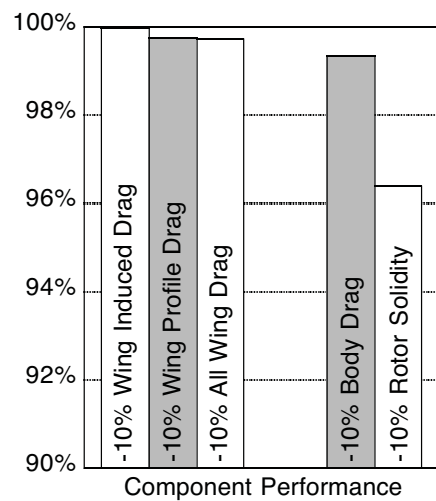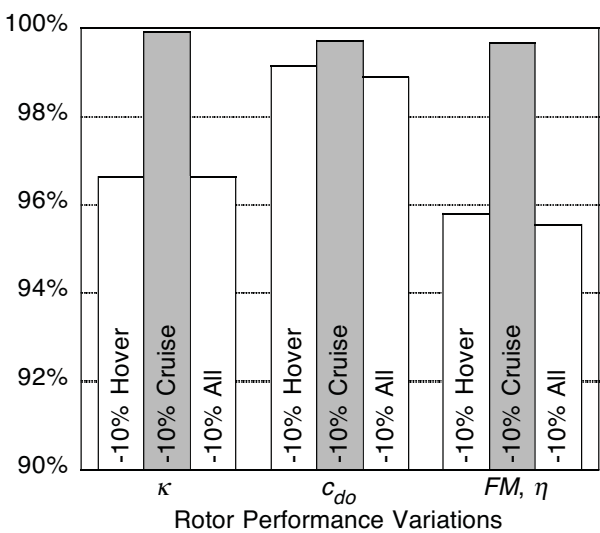
(a) Weight empty

(b) Mission fuel burn

(c) Installed power

Fig. 4. Impact of component performance improvements on LCTR2 design. Rotor drag effects are shown on the left; wing and fuselage drag and rotor lift effects are on the right.

Wing download was set to 90% of the nominal value, but the effect was negligible and is not presented here. At low speeds, the rotors carry most or all of the lift, so wing stall is not an issue. An increase in maximum wing lift has no effect on sizing and was accordingly not examined.

The largest improvement to overall vehicle efficiency results from higher blade loading, not higher rotor or wing efficiency (at least not as traditionally measured; see Ref. 28 for a different view of the matter). This leads to the paradox that maximizing rotor and wing efficiency may not result in the most efficient aircraft. In part this is because rotor and wing efficiency must be traded off against total vehicle L/D_e, and aerodynamic performance in general must be balanced against total weight. Higher C_{Tmax}/σ results in a smaller and lighter rotor, and lower profile drag and fuel consumption in cruise. A 10% increase in C_{Tmax}/σ would lead immediately to a 10% reduction in rotor weight, and a slightly greater reduction after resizing. The numerical calculations underlying Fig. 4 showed that figure of merit is barely affected, but η increases by 1.4%. Propagating these effects through mission analysis and sizing yield the net reductions in weight, power and fuel burn shown in Fig. 4.

Thus, a small, indirect improvement in η resulting from a smaller rotor is preferable to a much larger improvement for the same size rotor. Reduced rotor weight can easily be more valuable than improved figure of merit. Given also that C_{Tmax}/σ was set by turn performance, improvements to wing and rotor performance in turns might be a more productive avenue of future research than improvements to rotor efficiency, at least as traditionally defined in terms of figure of merit and propulsive efficiency.

Practical Considerations

The LCTR2 has to date been configured as a conventional tiltrotor with tilting nacelles and wing extensions. However, this potentially causes problems for ground handling. Collisions with ground vehicles is always a threat on the ramp, and is an important consideration in the structural design for airliners. Tilting the nacelles places the most expensive part of the aircraft—the engines—directly in harm's way.

Fixed nacelles and extensions, with only rotor shaft tilt, mitigate this problem. Furthermore, non-tilting extensions potentially have better low-speed turn performance, where the rotors provide much of the lift and must therefore be tilted nearly vertical. If a tilted extension is stalled, it acts as an airbrake; but if the rotor induced velocity is sufficient to keep the flow attached and prevent stall, the resulting section lift points rearwards, and again the extension acts as an airbrake. A fixed extension avoids both problems.

Tilting extensions may react strongly to crosswinds, with adverse consequences for handling qualities in hover (thanks to Tom Wood of Bell Helicopter for pointing this out).

LCTR2 spends little time in hover or at low speed, but improved handling qualities during OEI conditions are of obvious benefit even if only of short duration.

Fixed nacelles would have the further advantage of allowing swept extensions. If an extension of significant span and sweep tilts with the pylon, the tip will have inadequate ground clearance. Swept extensions potentially benefit aeroelastic stability. The Appendix to this paper summarizes the theoretical advantages. Reference 7 includes examples of whirl-flutter analyses with swept extensions. Swept extensions are included in the wing optimizations presented here, although no credit is taken for any stability improvements and associated weight reductions. The purpose is simply to show how sweep might be accommodated and included in the design process.

If the wing extensions were small enough, they could pivot independently of the nacelle, but at the cost of heavier structure plus the pivot actuators. For this reason, the extensions are assumed to be rigidly attached to the nacelles in the current design.

Wing Redesign

Based on the above considerations, the LCTR2 wing was redesigned with fixed extensions. Because of the limitations of the CAMRAD II lifting-line model, the Athena Vortex Lattice code (AVL, Ref. 22) was used to determine wing performance for a variety of parameter variations, including span, taper, sweep, and dihedral. Kinks in the lifting line, as would be introduced by sweep, will give inaccurate results in CAMRAD II. AVL can analyze wings with sweep and dihedral without difficulty. However, AVL cannot determine the effects of wing/rotor interactions.

The procedure used here was to separately compute isolated wing performance and wing/rotor interactions, then combine the results in the NDARC wing aerodynamic model. CAMRAD II computed wing performance, in terms of Oswald efficiency factor e, with and without interference. The difference due to interference was then added to the base value of e computed by AVL for an isolated wing, and the result input into NDARC for sizing. The wing drag coefficient was determined by CAMRAD II from airfoil tables.

Far more sophisticated analyses of combined wing/rotor performance are certainly possible; see in particular Ref. 6. AVL, however, has the compelling advantage of extremely fast execution, and is therefore preferred for basic sizing studies.

Table 3 compares four versions of the LCTR2 with wings designed to different criteria. All values in the table refer to fully resized aircraft. During resizing, the inner wing is scaled to maintain a 1.5-ft minimum clearance between the fuselage and rotor in airplane mode, and chord is adjusted to maintain wing loading, per Table 2.

Table 3. LCTR2 alternative wing designs.

	15 ft	15 ft	25 ft	0 ft
Extension Span:	15 ft	15 ft	25 ft	0 ft
Extension Sweep:	0	0	35 deg	0
Nacelle Tilt:	Yes	No	No	N/A
Gross weight, lb	82,975	83,537	86,266	81,812
Weight empty, lb	53,433	53,887	56,640	50,574
Rotor weight, lb (both rotors)	6362	6417	6687	6248
Wing weight, lb (zero fuel)	7358	7416	8984	4579
Extension weight, lb	1042	1047	1437	0
Engines and drive train, lb	9398	9588	9894	9637
[a]Fuselage empty weight, lb	10,892	10,948	11,216	10,778
Mission fuel burn, lb	8284	8401	8365	9980
Engine power, hp (MRP)	4×5549	4×5680	4×5871	4×5467
Rotor radius, ft	30.7	30.8	31.3	30.5
Hover FM	0.758	0.754	0.753	0.757
Cruise η	0.814	0.814	0.810	0.810
[b]Wing area, ft^2	790	796	822	779
[b]Wing span, ft	103.4	103.6	124.6	73.0
[b]Wing aspect ratio	13.5	13.5	18.9	6.84
Wing chord (inner), ft^2	8.44	8.47	7.85	10.67
[c]Wing efficiency e	1.09	1.09	1.05	1.08
Aircraft L/D	13.28	13.25	14.07	9.65
Drag D/q, ft^2	29.0	29.2	29.6	23.4

[a]Includes landing gear; [b]Includes extensions; [c]Includes interference

The baseline version (Fig. 1), with tilting nacelles and 15-ft extensions, is summarized in the first column. The baseline is the most fuel-efficient version studied, but suffers from ground handling and other limitations discussed in the previous section. The results for the baseline aircraft differ from those given in earlier publications because of several updates to the NDARC model, notably the addition of wing/rotor interference effects (Ref. 18). Revisions to the mission model climb specifications were mentioned previously. All results reported in Table 3 were fully resized with NDARC.

Also included in Table 3 are results for the original wing, but with fixed nacelles and wing extensions (second column). There are slight increases in weight, fuel burn, and installed power. The improved ground clearance provided by fixed nacelles costs about 1.4% in increased fuel burn. The traditional component efficiency metrics—figure of merit, propulsive efficiency, wing span efficiency (Oswald factor), and lift-to-drag ratio—are barely affected; the critical difference is higher download in hover.

A redesigned wing with longer, swept extensions is also included in Table 3 (third column); a planform view is shown in Fig. 5. This version is optimized for minimum mission fuel burn. The extension span is 25 ft per side, with a 20% taper ratio (tip chord/root chord) and 35-deg sweep; the sweep angle is derived in the Appendix. The fuel burn is less, but the larger extensions and increased download in hover result in larger engines and greater empty weight. Maintaining constant wing loading (Table 2) as span is increased results in a reduced inner wing chord, which emphasizes the apparent size of the extensions.

Adding dihedral or anhedral to the extensions provided no net benefit. Anhedral should improve handling qualities, but will reduce ground clearance. Reference 6 showed possible benefits from winglets, which are not considered here. Winglets reduce wing/rotor tip clearance in hover and would therefore require an additional design constraint.

The extensions are much lighter than the inner wing, because they do not carry the concentrated lift loads of the rotor, nor must they resist the destabilizing forces that cause whirl flutter. In consequence, wing area outboard of the rotor has a much lower weight cost than area inboard (about 16% of wing weight for 29% of the area). For the longer wing, figure of merit is barely affected, propulsive efficiency is very slightly less, and aircraft L/D is 6% greater. However, the narrower chord of the inner wing is structurally less efficient and the extension loads are greater, so the total wing weight increases by 21%. This plus the greater download in hover largely negates the benefits of a longer wing.

Fig. 5. LCTR with 25-ft swept extensions.

No credit is here taken for any aeroelastic benefit provided by the swept extensions. Fully integrated aerodynamic and aeroelastic optimization might reduce the wing weight, but is beyond the scope of the present study. The large amount of sweep shown in Fig. 3 had negligible effect on performance; it was retained here primarily to illustrate the possibilities of non-traditional layouts.

Table 3 also includes a design with no extensions at all (last column). This aircraft is the lightest studied, with the lowest power required, but its mission fuel burn is 20% greater than the baseline aircraft. Wing extensions are clearly beneficial for a long-range mission. Table 3 summarizes the penalties for a non-tilting layout.

The values of wing efficiency shown in Table 3 include wing/rotor interaction effects, and are therefore greater than unity. The long wing is inherently more efficient and does not benefit quite as much from the presence of the rotor.

The wing shown in Fig. 5 is not here proposed as realistic for production. It is unlikely that an airline would accept a 5% increase in empty weight for an 0.4% decrease in fuel consumption. A more severe criticism is that the longer wing exceeds the airport Group III wing span limit. Even longer extensions were examined, but provided no further benefit.

This design exercise, combined with the results of Fig. 4, illustrates that maximizing rotor and wing efficiency, or emphasizing fuel burn, may not result in the most effective aircraft.

Conclusions

Performance of the Large Civil Tiltrotor (LCTR2) was analyzed with ideal rotor, wing, and airframe aerodynamic performance; e.g., zero profile or excess induced drag, applied separately and in combination to the rotor, wing and airframe. Such assumptions represent the absolute physical limits of what a large tiltrotor might be capable of. The analysis was repeated with more realistic, if still highly ambitious, 10% improvements to aerodynamic performance, including maximum rotor lift (C_{Tmax}/σ). The LCTR2 was resized with NDARC, and empty weight, mission fuel burn, and installed power were compared.

Improved C_{Tmax} was more effective in reducing weight, power and fuel than any other single parameter. This result illustrates that maximizing traditional performance metrics such as wing efficiency (Oswald factor), rotor figure of merit, or propulsive efficiency may not result in the most effective aircraft. This further implies that turn performance may be a more important design driver than had been assumed and should be given at least equal priority to rotor hover or cruise performance. The development of a better NDARC model of turn performance is needed, which will require more extensive analyses of low-speed rotor and wing performance with CAMRAD II or other comprehensive code.

In conjunction with the idealized analyses, practical constraints on aircraft layout were also studied, here focused on non-tilting nacelles for better ground clearance. The opportunity was taken to introduce swept extensions, which have potential benefits for aeroelastic stability. Longer, more tapered extensions improved fuel burn, but at a significant cost in weight, power and ramp space. Again, maximizing performance does not guarantee a better airplane. Nevertheless, it may be possible to more fully exploit wing/rotor interactions for higher aerodynamic efficiency, especially if combined wing/rotor performance and wing/rotor aeroelastic stability (whirl flutter) can be simultaneously improved. Application of the methods of Ref. 6 or equivalent to further optimize the wing is recommended, as is a parallel effort to expand the work initiated in the Appendix to a more comprehensive study of passive enhancements to aeroelastic stability.

Appendix: Aerodynamic Damping of a Tiltrotor Wing with Extensions

To illustrate the potential benefits of wing-tip extensions for aeroelastic stability, a simple analysis of wing aerodynamic damping is presented here. Following Ref. 29, the modal equation can be written as

$$m_k \ddot{q} + \delta_k \dot{q} + k_k q = Q_{Ak}, \quad (1)$$

where m, δ and k are the modal mass, damping, and stiffness for mode k; q is the dimensionless mode shape; and Q_{Ak} is the generalized aerodynamic force.

Several simplifying assumptions are made in this analysis:

1) The wing and extension are constant chord (not necessarily equal) and unswept. A swept extension will be considered in a later section. Only a semi-span wing is considered here.

2) The mass of the system is dominated by the mass of the wing-tip nacelle, enough so that the mass of the extension can be neglected. This assumption is justifiable not only because a typical extension will be smaller than the wing, but also because the extension need not transfer rotor loads or nacelle inertial loads to the fuselage.

3) For the same reasons as assumption 2, modal deflections of the extension are negligible. The bending mode shape of the extension is assumed to be simply an extrapolation of the tangent to the inboard wing mode shape at the nacelle (Fig. A1), and the torsion mode shape is a constant angle equal to the inboard wing modal deflection at the nacelle.

4) Chordwise deflections have negligible effect on aerodynamic damping, or are small compared to the effects of perturbations in angle of attack caused by beamwise or torsional deflections.

5) For the inboard wing, the beam mode shape $\zeta(y)$ is quadratic, and the torsion mode shape $\gamma(y)$ is linear:

$$\zeta = \zeta_{tip}(y/b)^2$$

$$\gamma = \gamma_{tip}(y/b)$$

Outboard of the nacelle,

$$\zeta = \zeta_{tip} + (y-b)\frac{d\zeta}{dy}\bigg|_{y=b}$$

so

$$\zeta = \zeta_{tip}(2y/b - 1)$$

$$\gamma = \gamma_{tip}$$

The elastic motion is $\Delta z = \zeta q$ and $\Delta \phi = \gamma q$ for the bending and torsion modes, respectively.
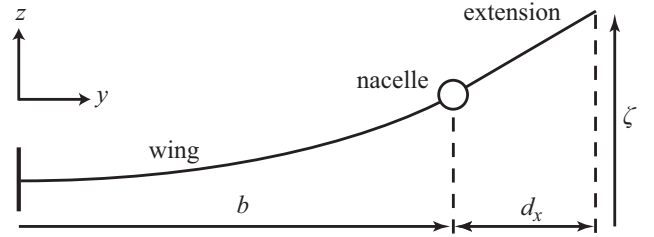

Fig. A1. Simplified bending mode shape for a semi-span wing with extension.

Aerodynamic forces

Following Ref. 29, the generalized aerodynamic damping force for mode k is

$$Q_{Ak} = -\frac{1}{2}\rho V^2 F_{q\dot{q}}(\dot{q}/V) \quad (2)$$

or in terms of the damping coefficient,

$$C_{Ak} = \frac{1}{2}\rho V F_{q\dot{q}}$$

The force coefficient is

$$F_{q\dot{q}} = \frac{d(Q_{Ak}/\frac{1}{2}\rho V^2)}{d(\dot{q}/V)}$$

For constant chord, the section lift is

$$L = \frac{1}{2}\rho V^2 \left[cc_{l_\alpha}\alpha + cc_{l_{\dot{\alpha}}}\left(\dot{\alpha}c/V\right) \right], \quad (3)$$

and $c_{l_\alpha} = 2\pi$ and $c_{l_{\dot{\alpha}}} = \frac{3}{2}\pi$ from thin-airfoil theory (Ref. 30).

For a wing trimmed to a small angle of attack and experiencing small modal deflections about the trimmed position,

$$\alpha = -\zeta\dot{q}/V \quad \text{and} \quad \dot{\alpha} = V\gamma\dot{q}/V$$

The section moment is

$$M = \frac{1}{2}\rho V^2 c^2 c_{m_{\dot{\alpha}}}\left(\dot{\alpha}c/V\right), \quad c_{m_{\dot{\alpha}}} = -\frac{\pi}{4} \text{ (Ref. 30)}.$$

$M(\alpha) = 0$ (or constant) over the assumed operating conditions.

Bending mode damping

For a pure bending mode, only the $\alpha = -\zeta\dot{q}/V$ contribution need be considered. Integrating equation (3) over the wing span,

$$Q_B = \int \zeta L\,dy = \int \zeta \frac{1}{2}\rho V^2 cc_{l_\alpha}\left(-\zeta\dot{q}/V\right)dy$$

Equating to Q_{Ak} (eqn. 2) gives

$$F_{q\dot{q}} = \int \zeta^2 cc_{l_\alpha}\, dy$$

For an extension with constant chord equal to that of the wing,

$$F_{q\dot{q}} = \left[\int_0^b \left(\zeta_{tip}(y/b)^2\right)^2 dy + \int_b^{b+d_x}\left(\zeta_{tip}(2y/b-1)\right)^2 dy\right] cc_{l_\alpha} \tag{4}$$

where d_x is the length of the extension; then,

$$\frac{F_{q\dot{q}}}{cc_{l_\alpha}} = \zeta_{tip}^2\left[\frac{b}{5} + d_x + \frac{2}{b}d_x^2 + \frac{4}{3}\frac{d_x^3}{b^2}\right]$$

Setting $d_x = 0$ gives the damping for the wing alone. If $d_x = b/3$, then the contribution to bending-mode damping by the extension is $(49/81)b = 0.605b$, or three times the contribution by the wing. Hence an extension with 1/3 the chord and 1/3 the length of the wing contributes the same bending-mode damping as the wing for 1/9 the area.

Torsion mode damping

For a pure torsion mode, only the $\dot{\alpha} = V\gamma \dot{q}/V$ contribution need be considered:

$$M(\dot{\alpha}) = \frac{1}{2}\rho V^2 c^2 c_{m_{\dot{\alpha}}}\left(\dot{\alpha}c/V\right)$$

$$Q_T = \int \gamma M(\gamma)\, dy = \int \gamma \frac{1}{2}\rho V^2 c^2 c_{m_{\dot{\alpha}}}\left(\gamma \dot{q}c/V\right)dy \tag{5}$$

For constant chord,

$$F_{q\dot{q}} = -\int \gamma^2 c^2 c_{m_{\dot{\alpha}}} c\, dy = \frac{\pi}{4}c^3 \int \gamma^2 dy \tag{6}$$

$$F_{q\dot{q}}\bigg/ \frac{\pi}{4}c^3 = \gamma_{tip}^2\left[\int_0^b \gamma_{tip}^2 (y/b)^2 dy + \int_0^{b+d_x}\gamma_{tip}^2 dy\right]$$

$$= \gamma_{tip}^2\left[\frac{b}{3} + d_x\right] \tag{7}$$

If $d_x = b/3$, then the contribution of the extension to torsion-mode damping is the same as the wing. An extension with 1/3 the span and 1/3 the chord of the wing, the same as for the bending-mode example, contributes 1/3 as much torsion-mode damping as the wing for 1/9 the area.

Offset extension damping

Assume the extension is offset aft by e_x. There is an additional moment due to the extension lift acting through the moment arm e_x. The elastic axes of the wing and extension are each assumed to coincide with the local aerodynamic center, shown in Fig. A2 at the ¼-chord line.
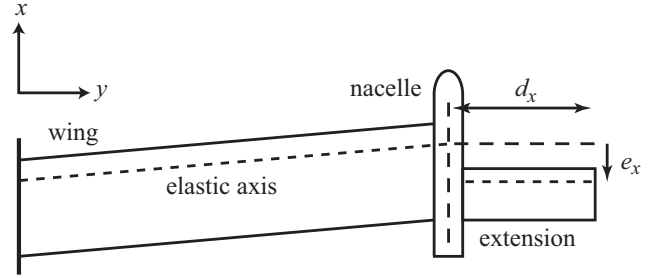

Fig. A2. Wing with offset extension.

The torsion mode damping force is

$$Q_T = \int \gamma M(\gamma)\, dy - \int \gamma e_x L(\gamma)\, dy - \int \zeta e_x L(\gamma)\, dy$$

(Note that positive lift creates a negative moment.)

The first term is identical to that derived in eqn. 5. For a pure torsion mode, the last term is zero. The remaining term due to offset has lift components arising from both vertical translation and rotation (pitching) of the offset airfoil:

$$Q_{Te_x} = \int \frac{1}{2}\rho V^2 \gamma e_x cc_{l_\alpha}\left(\zeta \dot{q}/V\right)dy - \int \frac{1}{2}\rho V^2 \gamma e_x c^2 c_{l_{\dot{\alpha}}}\left(\gamma \dot{q}/V\right)dy$$

Equating to Q_{Ak} (eqn. 2) gives

$$F_{q\dot{q}} = -e_x cc_{l_a}\int \gamma \zeta\, dy + e_x c^2 c_{l_{\dot{\alpha}}}\int \gamma^2 dy$$

The vertical and torsional deflections are $\zeta = -\gamma_{tip}e_x$ and $\gamma = \gamma_{tip}$, respectively, so the additional damping force is

$$F_{q\dot{q}} = e_x cc_{l_\alpha}\int_b^{b+d_x}\gamma_{tip}^2 e_x\, dy + e_x c^2 c_{l_{\dot{\alpha}}}\int_b^{b+d_x}\gamma_{tip}^2 dy$$

$$F_{q\dot{q}} = \gamma_{tip}^2 e_x^2 cc_{l_\alpha} d_x + \gamma_{tip}^2 e_x c^2 c_{l_{\dot{\alpha}}} d_x \tag{8}$$

The first term is the contribution from translation and the second term from pitching.

Substituting $c_{l_\alpha} = 2\pi$ and $c_{l_{\dot\alpha}} = \frac{3}{2}\pi$,

$$F_{q\dot q} = \gamma_{tip}^2 e_x^2 c 2\pi d_x + \gamma_{tip}^2 e_x c^2 \frac{3}{2}\pi d_x$$

$$F_{q\dot q} = \gamma_{tip}^2 e_x c\pi d_x \left(2e_x + c\frac{3}{2}\right)$$

This is the additional torsion-mode damping contributed by the offset; compare equation (7).

Assume $d_x = b/3$ and $e_x = c/2$:

$$F_{q\dot q} = \gamma_{tip}^2 \left(\frac{c}{2}\right)^2 c2\pi \frac{b}{3} + \gamma_{tip}^2 \frac{c}{2}c^2 \frac{3}{2}\pi \frac{b}{3}$$

$$F_{q\dot q}\left/\frac{\pi}{4}c^3\right. = \gamma_{tip}^2 b\left(\frac{2}{3}+1\right)$$

Thus the additional contribution of the extension offset to torsion-mode damping is 5 times greater than that of either the extension alone or the wing alone. An extension with 1/3 the span and 1/3 the chord of the wing, offset aft by 1/2 the wing chord, contributes twice as much torsion-mode damping as the wing for 1/9 the area.

Sweep

If the extension is swept instead of offset, the moment arm e_x will be proportional to the sine of the sweep angle Λ. For constant extension chord,

$$e_x = \frac{1}{2}d_x \sin\Lambda$$
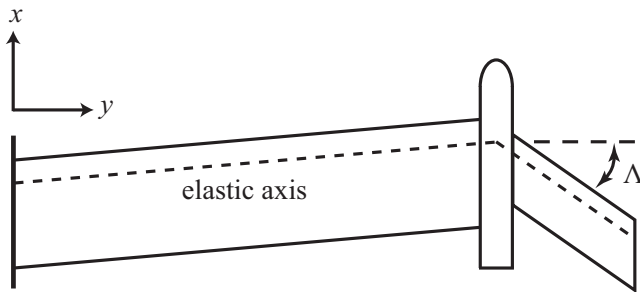

Fig. A3. Wing with swept extension.

The aerodynamic coefficients will be proportional to $\cos^2\Lambda$,

e.g., $c_{l_\alpha} = 2\pi \cos^2\Lambda$

Substituting into equations (4), (6) and (8) yields formulae with terms in b, c, d_x, ζ, γ, and Λ. The value of sweep that maximizes damping will depend on all of these terms, plus taper if present. Hence aerodynamic optimization is intimately linked to structural optimization, which is not considered here.

An approximate value for optimum Λ can be readily obtained by maximizing the product $\sin\Lambda\cos^2\Lambda$, which yields $\tan\Lambda = \sqrt{\frac{1}{2}}$, or $\Lambda = 35$ deg. This is the value of sweep chosen for the analyses in this paper, pending structural re-optimization of the wing.

Figure A3 shows the elastic axes of the wing and extension intersecting at the center of the nacelle, on the grounds that this minimizes the load path to the nacelle pivot spindle. Combining sweep and offset for greater pitch damping is possible, but at the expense of greater weight in the nacelle carry-through structure.

Limitations

Actual wing modes will typically have beamwise, chordwise, and torsional components, which must be combined to get the net damping. In the complete solution, the aerodynamic damping matrix will have off-diagonal terms. The effectiveness of the extension will depend upon aspect ratio, endplate effect of the nacelle, nonlinear aerodynamics, anhedral, and other design features not considered here. The net effect on the aeroelastic stability margin will depend upon the detailed mode shapes of the wing/nacelle modes.

An important consideration is that for fully coupled mode shapes, the net effect of an offset or swept extension may not be beneficial for all modes. The quasi-steady aerodynamic force on the extension caused by upwards wing bending will tend to pitch the nacelle nose up; that is, the aerodynamic spring effect can be negative, with an off-diagonal term. For whirl-mode stability, the net deflection at the rotor hub is the critical parameter, whereas all damping values derived here assume deflections relative to the wing elastic axis. A bend-up, pitch-up coupling is therefore detrimental. The relative amounts of bending and pitching deflections for the worst-case mode will determine whether sweep is beneficial.

Additional analysis, or direct modeling with a comprehensive aeromechanics code, is needed to determine the net effect of all such couplings for a particular design.

References

1. Johnson, W., Yamauchi, G. K., and Watts, M. E., "NASA Heavy Lift Rotorcraft Systems Investigation," NASA TP-2005-213467, September 2005.

2. Acree, C. W., "Integration of Aeromechanics Analysis with the Conceptual Design of a Large Civil Tiltrotor," AHS Aeromechanics Specialists' Conference, San Francisco, California, January 2010.

3. Acree, C. W., Yeo, H., and Sinsay, J. D., "Performance Optimization of the NASA Large Civil Tiltrotor," International Powered Lift Conference, London, UK, July 2008; also NASA TM-2008-215359, June 2008.

4. Acree, C. W. and Snyder, C. A., "Influence of Alternative Engine Concepts on LCTR2 Sizing and Mission Profile," AHS Future Vertical Lift Aircraft Design Conference, San Francisco, California, January 2012.

5. Snyder, C. A.; Acree, C. W., "Assessing Variable Speed Power Turbine Technology on LCTR2 Size and Performance," American Helicopter Society 68th Annual Forum, Fort Worth, Texas, May 2012.

6. Cole, J. A., Maughmer, M. D., and Bramesfeld, G., "Aerodynamic Design Considerations for Tiltrotor Wing Extensions and Winglets," AIAA-2013-1088, 51st AIAA Aerospace Sciences Meeting, Grapevine, Texas, January 2013.

7. Zhang, J. and Smith, E. C., "Influence of Aeroelastically Tailored Wing Extensions and Winglets on Whirl Flutter Stability," 2nd Asian/Australian Rotorcraft Forum and 4th International Basic Research Conference on Rotorcraft Technology, Tianjin, China, September 2013.

8. Jones, W. T., Nielsen, E. J., Lee-Rausch, E. M., and Acree, C. W., "Multi-point Adjoint-Based Design of Tilt-Rotors in a Noninertial Reference Frame," AIAA Science and Technology Forum and Exposition, National Harbor, Maryland, January 2014.

9. Theodore, C. R., Willink, G. C., Amy, A. R., Russell, C. R., and Pete, A. E., "Wind Tunnel Testing of a 1/20th Scale Large Civil Tilt-Rotor Model in Airplane and Helicopter Modes," Fifth Decennial AHS Aeromechanics Specialists' Conference, San Francisco, California, January 2014.

10. Schillings, J. J., Roberts, B. J., Wood, T. L., and Wernicke, K. G., "Maneuver Performance of Tiltrotor Aircraft," AHS 43rd Annual Forum Proceedings, St. Louis, Missouri, May 1987 (Rev. June 1987).

11. McEntire, K., "XV-15 Full Scale Test Data Correlation Report," Bell report 901-909-003, November 1985.

12. Arrington, W. L., Kumpel, M., Marr, R. L., and McEntire, K. G., "XV-15 Tilt Rotor Research Aircraft Flight Test Data Report, Vol. II," NASA CR-177406, USAAVSCOM TR-86-A-1, June 1985.

13. Yeo, H., Sinsay, J. D., and Acree, C. W., "Blade Loading Criteria for Heavy Lift Tiltrotor Design," AHS Southwest Region Technical Specialists' Meeting on Next Generation Vertical Lift Technologies, Dallas, Texas, October 2008.

14. Russell, C. and Johnson, W., "Conceptual Design and Mission Selection for a Large Civil Compound Helicopter," AHS Future Vertical Lift Aircraft Design Conference, San Francisco, California, January 2012.

15. Robuck, M., Wilkerson, J., Zhang, Y., Snyder, C. A., and Vonderwell, D., "Design Study of Propulsion and Drive Systems for the Large Civil TiltRotor (LCTR2) Rotorcraft," AHS 67th Annual Forum Proceedings, Virginia Beach, Virginia, May 2011.

16. Snyder, C. A. and Thurman, D. R., "Effects of Gas Turbine Component Performance on Engine and Rotary Wing Vehicle Size and Performance," AHS 66th Annual Forum Proceedings, Phoenix, Arizona, May 2010.

17. Snyder, C. A., "Defining Gas Turbine Engine Performance Requirements for the Large Civil Tiltrotor (LCTR2)," AHS 67th Annual Forum Proceedings, Virginia Beach, Virginia, May 2011.

18. Johnson, W., "NDARC, NASA Design and Analysis of Rotorcraft," NASA TP 2009-215402, December 2009.

19. Johnson, W., "NDARC—NASA Design and Analysis of Rotorcraft: Theoretical Basis and Architecture," AHS Aeromechanics Specialists' Conference, San Francisco, California, January 2010.

20. Johnson, W., "NDARC—NASA Design and Analysis of Rotorcraft: Validation and Demonstration." AHS Aeromechanics Specialists' Conference, San Francisco, California, January 2010.

21. Johnson, W., "Rotorcraft Aerodynamics Models for a Comprehensive Analysis," AHS 54th Annual Forum Proceedings, Washington, D.C., 1998.

22. Drela, M. and Youngren, H., "AVL 3.30 User Primer," http://web.mit.edu/drela/Public/web/avl/, August 2010.

23. Jones, S. M., "An Introduction to Thermodynamic Performance Analysis of Aircraft Gas Turbine Engine Cycles Using the Numerical Propulsion System Simulation Code," NASA/TM-2007-214690, March 2007.

24. Tong, M.T. and Naylor, B.A., "An Object-Oriented Computer Code for Aircraft Engine Weight Estimation," GT2008-50062, ASME Turbo-Expo 2008, Berlin, Germany, June 2008.

25. Kroo, I., "Propeller-Wing Integration for Minimum Induced Loss," *Journal of Aircraft*, Vol. 23, No. 7, July 1986.

26. McVeigh, M. A., Grauer, W. K., and Paisley, D. J., "Rotor/Airframe Interactions on Tiltrotor Aircraft," AHS 44th Annual Forum Proceedings, Washington, D.C., June 1988.

27. Yeo, H. and Johnson, W., "Performance and Design Investigation of Heavy Lift Tiltrotor with Aerodynamic Interference Effects," AHS 63rd Annual Forum Proceedings, Virginia Beach, Virginia, May 2007.

28. Leishman, J. G. and Rosen, K. M., "Challenges in the Aerodynamic Optimization of High-Efficiency Proprotors," American Helicopter Society 65th Annual Forum, Grapevine, Texas, May 2009.

29. Johnson, W., *Comprehensive Analytical Model of Rotorcraft Aerodynamics and Dynamics, Vol. II: Components Theory*, Chapter 5, Johnson Aeronautics, Palo Alto, California, 2007.

30. Bisplinghoff, R. L., Ashley, H., and Halfman, R. L., *Aeroelasticity*, p. 279, Addison-Wesley, 1955.